Biophysical Journal Volume 75 July 1998 41–52

Structure of the Ca^{2+} Pump of Sarcoplasmic Reticulum: A View along the Lipid Bilayer at 9-Å Resolution

Haruo Ogawa,*# David L. Stokes,§ Hiroyuki Sasabe,¶ and Chikashi Toyoshima*

*Institute of Molecular and Cellular Biosciences, University of Tokyo, Bunkyo-ku, Tokyo 113, Japan; #Department of Biological Sciences, Tokyo Institute of Technology, Midori-ku, Yokohama 226, Japan; §Skirball Institute of Biomolecular Medicine, New York University Medical Center, New York, New York 10016, USA; and ¶Frontier Research Program, RIKEN, Wako, Saitama 351-01, Japan

ABSTRACT We have used multilamellar crystals of the ATP-driven calcium pump from sarcoplasmic reticulum to address the structural effects of calcium binding to the enzyme. They are stacks of disk-shaped two-dimensional crystals. A density map projected along the lipid bilayer was obtained at 9-Å resolution by frozen-hydrated electron microscopy. Although only in projection, much more details of the structure were revealed than previously available, especially in the transmembrane region. Quantitative comparison was made with the model obtained from the tubular crystals of this enzyme formed in the absence of calcium. Unexpectedly large differences in conformation were found, particularly in the cytoplasmic domain.

INTRODUCTION

Calcium ATPase (Ca^{2+}-ATPase) of the sarcoplasmic reticulum (SR) is an integral membrane protein of M_r 110,000. It pumps calcium ions from the cytoplasm into the SR against a large concentration gradient, thereby causing the relaxation of muscle cells. It is a member of P-type ion pumps that include Na^+K^+-ATPase and H^+K^+-ATPase (for a recent review, see Møller et al., 1996). The amino acid sequence has been determined for many species (MacLennan et al., 1985; Brandl et al., 1986), and extensive predictions of the secondary structure have been made (Brandl et al., 1986; Taylor and Green, 1989). Site-directed mutagenesis studies have identified four critical amino acid residues implicated in calcium transport, all on putative transmembrane helices (Clarke et al., 1990; Chen et al., 1996; Rice and MacLennan, 1996). Hence it is generally believed that calcium ions bind directly to the high-affinity sites located within the membrane. The binding of calcium ions induces conformational changes in the ATP-binding site, resulting in ATP hydrolysis and phosphorylation of the enzyme. The phosphorylation, in turn, causes conformational changes in the calcium-binding site, and the enzyme eventually transfers two calcium ions into the lumen of SR per ATP molecule hydrolyzed (for a review see, e.g., Inesi, 1994).

Many studies have characterized these conformational changes by various techniques (reviewed by Bigelow and Inesi, 1992; Martonosi, 1995). For example, fluorescein isothiocyanate attached near the ATP binding site (Pick and Karlish, 1980) and affinity labeling of the ATP binding site (Yamamoto et al., 1989) have been used to determine that conformational changes do occur around the ATP binding site when Ca^{2+} binds to the high affinity site. Nevertheless, hardly any changes in the secondary structure have been detected, suggesting that the conformational changes are segmental movements (Csermely et al., 1987; Nakamoto and Inesi, 1986; Girardet and Dupont, 1992). Profile x-ray diffraction studies have demonstrated that long-range structural changes occur with flash photolysis of caged calcium (DeLong and Blasie, 1993), but this method can only detect movements normal to the membrane. Therefore, direct visualizations are clearly needed to determine the magnitude of these conformational changes and to understand how the binding signal at one site is transmitted to the other.

Calcium ATPase from rabbit skeletal muscle SR can be crystallized in several forms suitable for cryoelectron microscopy (for a review see, e.g., Martonosi, 1995). Two-dimensional ordering within the native membrane can be induced by either lanthanides (Dux et al., 1985) or vanadate (Dux and Martonosi, 1983). The three-dimensional structure has been determined at 14-Å resolution with the tubular crystals induced by vanadate in the absence of calcium (Toyoshima et al., 1993a). With enzymes solubilized and reconstituted into lipid bilayers, multilamellar three-dimensional microcrystals have been obtained (Dux et al., 1987; Stokes and Green, 1990a). These crystals are stacks of two-dimensional sheets formed in a high concentration of calcium ions; therefore, the enzyme in this type of crystal must be in a physiological state different from that in the tubular crystals (Dux et al., 1987; Stokes and Lacapère, 1994).

With these crystals, the direction of crystal growth can be adjusted by changing the lipid:protein:detergent ratio (Stokes and Green, 1990b; Cheong et al., 1996). It is possible to make the long axis of the crystal normal to the lipid bilayers. Because such crystals appear like worms, they show many different views on microscope grids roughly in the direction parallel to the lipid bilayer. Nevertheless, the

Received for publication 6 August 1997 and in final form 17 April 1998.

Address reprint requests to Dr. C. Toyoshima, Institute of Molecular and Cellular Biosciences, University of Tokyo, Bunkyo-ku, Tokyo 113, Japan. Tel.: 81-3-3814-6347; Fax: 81-3-5689-7227; E-mail: ct@iam.u-tokyo.ac.jp.

Dr. Ogawa's present address is Institute for Brain Research, School of Medicine, University of Tokyo, 7-3-1 Hongo, Bunkyo-ku, Tokyo 113, Japan.

0006-3495/98/07/41/12 $2.00

view along the *b* axis (shown in Fig. 1) was the one most frequently identified, and projection maps at low resolution have been published (Stokes and Green, 1990b; Cheong et al., 1996). We managed to collect six such images that diffracted to better than 10-Å resolution and describe here a side view of Ca^{2+}-ATPase in the presence of calcium. We also quantitatively compared the projection map with those calculated from the tubular crystals to visualize the conformational changes caused by the binding of calcium ions to the enzyme.

MATERIALS AND METHODS

Preparation and crystallization of Ca^{2+}-ATPase

SR was prepared from white skeletal muscles of rabbit legs as described by Champeil et al. (1978). Calcium ATPase was affinity purified with red agarose (Reactive Red 120 from Sigma Chemical Co.) as described by Coll and Murphy (1984). A small amount of phospholipid was supplemented during the purification procedure. Crystallization was carried out essentially as described previously (Stokes and Green, 1990a).

ATPase activity

The ATPase activity of the enzyme preparation was measured at 25°C by a coupled enzyme method (Anderson and Murphy, 1983). Final concentrations in 800 μl assay solution were 5 μg of Ca^{2+}-ATPase, 2 mM ATP, 65 mM 3-(*N*-morpholino)propanesulfonic acid (pH 7), 130 mM KCl, 6 mM $MgCl_2$, 0.13 mM $CaCl_2$, 0.5 mM phosphoenolpyruvate, 1 mg/ml $C_{12}E_8$, 0.2 mM NADH, 24 units pyruvate kinase, and 18 units lactic dehydrogenase.

Electron microscopy

Before rapid freezing, the solution containing microcrystals was dialyzed for 2 h against the crystallization buffer, with no glycerol to reduce the concentration of glycerol. This dialysis was necessary to prevent too much solution from being left on the specimen grids after blotting with filter paper. The specimen solution was deposited on carbon-coated holey grids. Blotting from the side of the grid opposite that to which the specimen solution was applied (Toyoshima, 1989) was necessary to retain a sufficient amount of crystals on the grid.

The specimen was rapidly frozen in ethane slush and kept in liquid nitrogen until use. The specimen grids were mounted on a Gatan 626 cryoholder and examined in a JEOL JEM2000EX microscope operated at 200 kV accelerating voltage. A double-blade anticontaminator (Gatan 651-N) was always in place. All of the images were taken at a nominal magnification of 40,000× with the minimal dose system and recorded on Kodak SO163 film. The objective lens current was monitored. The magnification was calibrated using negatively stained tropomyosin tactoids (Caspar et al., 1969) at various objective lens currents.

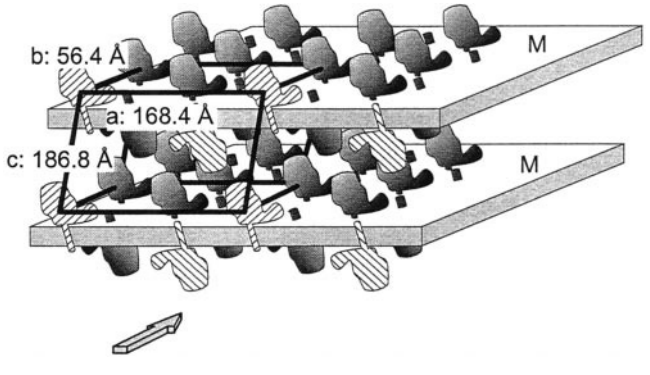

FIGURE 1 A cartoon depicting the configuration of the multilamellar crystals of Ca^{2+}-ATPase. The protein molecules are protruding from both sides of the bilayers (M) that contain lipids and, presumably, detergents. This type of three-dimensional crystal is essentially a stack of two-dimensional crystals. The enzyme molecules are arranged in a C2 lattice with twofold rotation axes parallel to the *b* axis (along the membrane plane). The unit cell dimensions are $a = 168.4$ Å, $b = 56.4$ Å, $c = 186.8$ Å; $\alpha = 90°$, $\beta = 83.9°$, $\gamma = 90°$. The arrow corresponds to the viewing direction of the electron micrograph in Fig. 2 *a*.

Image analysis

Images were first selected by optical diffraction, and those that gave clear spots beyond 10-Å resolution were digitized. The densitometer used was an Orbital Science 1010M with spot size and scanning intervals of 10 μm × 10 μm. Digitized images were analyzed by the established way for two-dimensional crystals (Amos et al., 1982), including distortion corrections of the crystal lattice (Henderson et al., 1986).

Because electron diffraction was not feasible with the multilamellar crystals, compensation of Fourier amplitudes for the uneven contrast transfer function (CTF) was necessary. This requires accurate determination of defocus parameters from micrographs. At first, defocus parameters were estimated from the locations of the Thon rings arising presumably from disordered phospholipids in the multilamellar crystals, by using a set of programs described elsewhere (Tani et al., 1996). Here the amplitude contrast of 4.8% was assumed (Toyoshima et al., 1993b). Then the Fourier terms from various images were averaged to make a preliminary reference data set, taking the CTF information thus obtained into account. In the next step, defocus parameters were refined by fitting the Fourier terms from each image to the preliminary reference data set compensated for the averaged CTF. In the fitting process, both amplitude variations and phase reversals due to the CTF were examined. These procedures were iterated several times to obtain the final averaged Fourier terms. No temperature factor compensation (Schertler et al., 1993) was introduced. Only the effects of the modulation transfer function of the emulsion and the densitometer were compensated for as described by Downing and Grano (1982). In fitting and averaging various images, the envelope function of the CTF was calculated for each image and was used as a weighting function.

Correlation calculation

To calculate correlation functions, a monomer was cut from the three-dimensional model of the tubular crystals (Toyoshima et al., 1993a). The density cutoff level for the model was chosen so that ~100% of the expected volume was recovered (assuming an M_r of 110K and a partial specific volume of 0.74 cm^3/g, based on the amino acid composition). The cut out monomer was then rotated and projected in a desired direction. The average density along the perimeter of the projected molecule was subtracted for floating. Care was taken to match the average densities of the two maps to be compared. Correlation functions were then calculated in reciprocal space, using the data to 14-Å resolution, so that the two structures were compared at the same resolution. The top view (Fig. 5, *a* and *c*) of the multilamellar crystals was calculated from the published data (Stokes and Green, 1990a), with a resolution limited to 14 Å. When correlation was to be maximized using the top views, two possibilities for the viewing direction of a projection were also examined. Correlation functions for top views were also calculated in real space with an MRC program, IMROTRAN.

RESULTS

A view of multilamellar crystals of Ca^{2+}-ATPase along the plane of the lipid bilayer

Multilamellar crystals of calcium ATPase reconstituted into lipid bilayers were formed in the presence of 10 mM calcium at pH 6 (Stokes and Green, 1990a,b). When the lipid-to-protein ratio was decreased, they tended to grow principally normal to the lipid bilayer and sometimes formed large stacks of two-dimensional crystals (Fig. 1; Stokes and Green, 1990a; Cheong et al., 1996). The packing model for the multilamellar crystals is shown in Fig. 1 (Taylor et al., 1988; Stokes and Green, 1990b; Cheong et al., 1996). Because these multilamellar crystals consist of disk-shaped membranes, they showed many different views on the microscope grids. Occasionally double bands of lipid bilayers and stripes of protein densities were clearly seen to be running slightly inclined from normal to these bands (Fig. 2 *a*). From the lattice parameters, these images were thought to correspond to the views along the *b* axis of the crystals (Fig. 1; Cheong et al., 1996). They diffracted to better than 10-Å resolution, as demonstrated by the computer transform (Fig. 2 *b*). We collected six such images and averaged them in Fourier space. Merging statistics were good up to 7-Å resolution, but the twofold phase residual was not so good at high resolution (Table 1). This may be a result of the orientation of the crystals, such that the direction of view is slightly offset from the *b* axis.

The projection map calculated at 9-Å resolution (Fig. 3) showed several distinct features and more details than previously available (Stokes and Green, 1990b; Cheong et al., 1996). Because of possible overlap of neighboring molecules (e.g., two molecules within the unit cell in Fig. 3) pointing in opposite directions, the boundary between neighboring enzyme molecules is ambiguous in some parts, particularly around the lipid bilayer. Nevertheless, it is obvious that the "head" piece of the cytoplasmic domain consists of two well-separated domains that are different in size, and that the transmembrane region consists of at least three columns (numbered in Fig. 3), presumably composed of bundles of α-helices. All transmembrane columns were inclined by ~30° from vertical (normal to the membrane plane). At this stage it is not clear whether column 3 belongs to the same molecule or to the adjacent one. The larger cytoplasmic domain (HL) consists of two barely resolved subdomains of nearly equal density, each of which appears to be connected to the transmembrane column 2 by a thin rod (*short bars* in Fig. 3). The smaller domain (HS) appears to have only a tenuous connection with the transmembrane region and an even weaker one with the larger cytoplasmic domain (HL).

The split appearance of the cytoplasmic domains of the enzyme in the multilamellar crystals is the most conspicuous feature and is in marked contrast with those in the tubular crystals, which constitute a single entity that looks like the head of a bird (Fig. 4, *a* and *b*; Toyoshima et al., 1993a). The split appearance cannot be a result of overlap of enzyme molecules in the crystal lattice (Fig. 1) or an effect of improved resolution (9 Å in Fig. 3, instead of 14 Å with tubular crystals). The corresponding image from the multilamellar crystals calculated at 14-Å resolution (Fig. 5 *b*) also showed a clear groove between the larger and smaller domains on the cytoplasmic

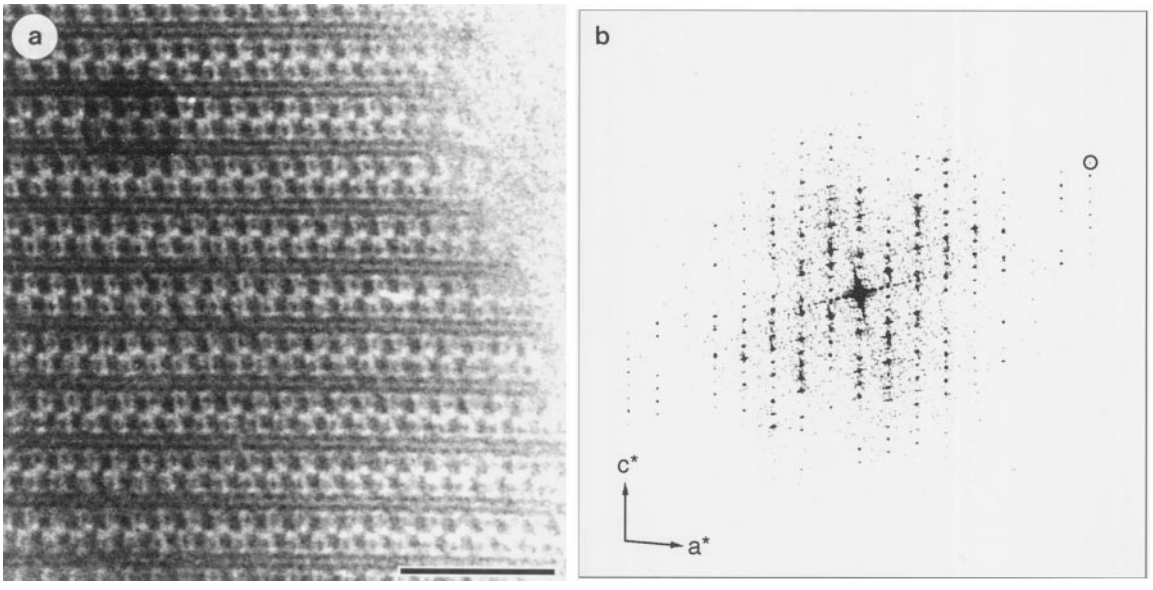

FIGURE 2 (*a*) Electron micrograph of a multilamellar crystal of Ca^{2+}-ATPase exhibiting the view along the *b* axis. The arrangement of the enzyme molecules in the crystal and the viewing direction are illustrated in Fig. 1. Note that the two leaflets of the lipid bilayers are clearly seen. The specimen is suspended in amorphous ice stretched over a hole in the carbon support film. The scale bar corresponds to 500 Å. (*b*) Diffraction amplitudes of a less defocused image of the crystal shown in *a*. The orientations of the *a** and *c** axes are indicated. The strong reflection at 1/9.1 $Å^{-1}$ (with a signal-to-noise ratio of 11.8) is circled. This particular transform appears anisotropic because the image was recorded at a small defocus (3400 Å) with a large amount of astigmatism (4160 Å).

TABLE 1 Statistics of electron crystallographic data*

Resolution range (Å)	No. of used reflections	Completedness (%)	Figure of merits[#]	Modified figure of merits[§]	Merging phase residuals[¶] (°)	Twofold phase residuals[‖] (°)
~15	109	100.0	0.915	0.816	15.9	8.2
15–12	42	70.0	0.848	0.664	26.7	26.0
12–9	82	62.6	0.844	0.597	28.8	36.8
9–7	92	48.4	0.855	0.573	24.4	40.7

*Only the spots whose signal-to-noise ratio was higher than 2 after merging and to which at least two images contributed were used for this table.
[#]The figure of merit for a reflection is defined as

$$\frac{|\sum \mathrm{CTF}\cdot \boldsymbol{F}_{\mathbf{obs}}|}{\sum|\mathrm{CTF}\cdot \boldsymbol{F}_{\mathbf{obs}}|}$$

where CTF is the value of the contrast transfer function, and $\boldsymbol{F}_{\mathbf{obs}}$ is the observed Fourier term. This is a conventional figure of merit and is not useful for determining the resolution limit when a relatively small and variable number of images contribute to the average. The value is 0 if the phases are random, 1 if the phases are the same or only one image contributes. The summations are taken over the images contributing to the same reflection.
[§]The modified figure of merit is defined as

$$\frac{|\sum S/N\cdot \mathrm{CTF}\cdot \boldsymbol{F}_{\mathbf{obs}}|}{\sum S/N\cdot|\mathrm{CTF}\cdot \boldsymbol{F}_{\mathbf{obs}}|}\cdot\sqrt{\frac{N_s-1}{N_{\max}}}$$

where S/N refers to the signal-to-noise ratio of the observed reflection, $N_{\max}$ is the maximum number of images constituting the data set, N_s is the number of images actually contributing to the reflection ($N_s \le N_{\max}$). This kind of figure of merit is useful when a relatively small and variable number of images contribute to the average. The value becomes very close to 1 when N_s is large and the phases are the same. The value becomes smaller if the number of contributing images becomes smaller. The value is 0 if only one image contributes (i.e., $N_s = 1$) or if the phases are random. The summations are taken as described in the table footnote above on the definition of the figure of merit for a reflection.
[¶]The merging phase residual for a reflection is defined as

$$\frac{\sum|\mathrm{CTF}\cdot \boldsymbol{F}_{\mathbf{obs}}|\cdot|\phi_{\mathrm{avg}}-\phi|}{\sum|\mathrm{CTF}\cdot \boldsymbol{F}_{\mathbf{obs}}|}$$

where ϕ_{avg} represents the averaged phase, and ϕ the phase of individual transform. The summations are taken as described in the footnotes above.
[‖]Twofold phase residuals can be used as a measure of data quality, because twofold rotation axes exist parallel to the *b* axis of the crystal (normal to the image). A twofold phase residual for a reflection is defined as

$$\frac{\sum|\mathrm{CTF}\cdot \boldsymbol{F}_{\mathbf{obs}}|\cdot|\phi_{2\,\mathrm{fd}}-\phi|}{\sum|\mathrm{CTF}\cdot \boldsymbol{F}_{\mathbf{obs}}|}$$

where $\phi_{2\mathrm{fd}}$ refers to the ideal phase expected from a twofold symmetry (either 0° or 180°, whichever is closer), and ϕ is the phase of individual transform. The summations are taken as described in the footnotes above.

side; at this resolution two transmembrane columns (1 and 3) could not be resolved (Fig. 5 *b*).

Comparison with the structure of Ca^{2+}-ATPase in the tubular crystals

To make a quantitative comparison with the structure of the enzyme in the absence of calcium, monomers of Ca^{2+}-ATPase were cut out from the three-dimensional model (Toyoshima et al., 1993a) of the tubular crystals (hereafter referred to as the 3D model) and arranged in various configurations to match the densities in the projection map from the multilamellar crystals. To do so, we used two projection maps of the multilamellar crystals in (nearly) orthogonal directions, one projected perpendicular to the membrane (top view, Fig. 5 *a*; Stokes and Green, 1990a), and the other projected along the plane of the lipid bilayer (side view, Fig. 5 *b*). Both were calculated at the same resolution (14 Å) as that of the structure from the tubular crystals, to avoid the effects of difference in resolution.

Because the direction of the lipid bilayer in the multilamellar crystals was already known, only one rotational parameter (in the plane of the lipid bilayer) and three translational parameters had to be determined. It was more straightforward to start with the top view, because the rotational and the two translational parameters could be determined directly. Therefore, the 3D model was first projected normal to the membrane (Fig. 4 *c*) and was correlated with the corresponding projection map of the multilamellar crystals. In Fig. 5 *c* is a composite of the 3D model (in *red*) superimposed on the projection map (top view) of the multilamellar crystal (in *green*) at the best fitting position. The correlation function showed a broad peak when plotted against the azimuthal angle. If the center of the peak was chosen for the azimuth, that is, if the 3D model was rotated by 4° counterclockwise from that shown in Fig. 4 *c*, the matching of the densities was reasonably good (Fig. 5 *c*).

The next step was to find the third translational parameter in the plane perpendicular to the lipid bilayer. To do so, the

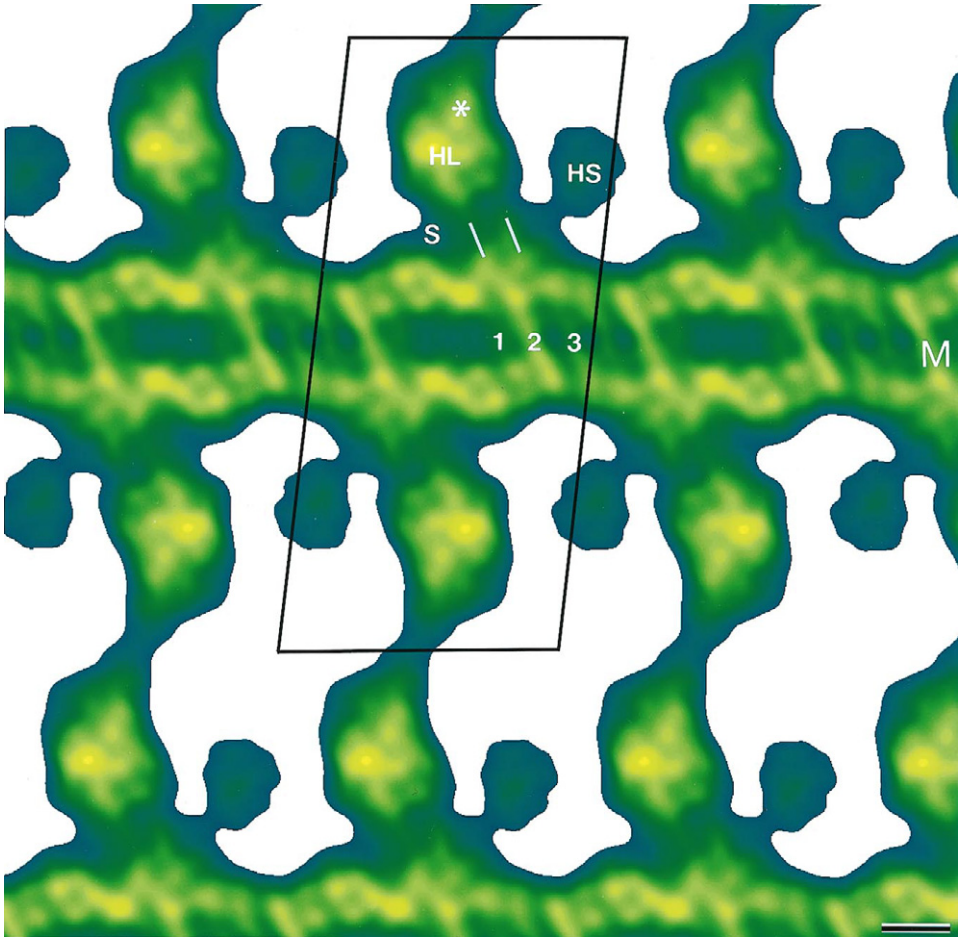

FIGURE 3 A projection map along the *b* axis of a multilamellar crystal of Ca^{2+}-ATPase, with the *a* axis horizontal. The map was calculated at 9-Å resolution from the data set averaged over six images; all of the reflections were used if the signal-to-noise ratio was higher than 2 after averaging. Note that the cytoplasmic region consists of two well-separated densities (HL and HS), and the transmembrane region (M) of at least three columns (1, 2, and 3) inclined by ~30° from vertical. HL domain is connected to the membrane region through a stalk (S), which consists of two thin rods (*short bars*). One unit cell is enclosed (*a*-axis dimension is one half of that of the three-dimensional unit cell specified in Fig. 1). The asterisk denotes a subsidiary peak in HL domain (see Fig. 7). The scale bar corresponds to 20 Å.

3D model was projected in the direction corresponding to the *b* axis of the multilamellar crystals, and the projection map was calculated (in *red* in Fig. 5 *d*); then it was correlated with the side view of the multilamellar crystals (in *green* in Fig. 5 *d*). The projection maps that gave the highest correlation are shown superimposed (Fig. 5 *d*). Note that the overlap of the 3D models is correctly displayed only between the short vertical bars at the top of the figure (Fig. 5 *d*).

It is clear in Fig. 5 *d* that both the cytoplasmic and the membrane domains of the multilamellar crystals (*green*) are markedly different from those of the 3D model (*red*). Confirming the visual impression, the connection between the smaller cytoplasmic domain (HS) and the larger one (HL) is strong in the 3D model (*red*), but nearly lost in the multilamellar crystals (*green*). Although the positions of the stalk (*short white bars* in Fig. 3) roughly coincide, the larger cytoplasmic domain (HL) appears to be offset by ~14 Å horizontally. In the transmembrane region, the difference is conspicuous around the position marked by the open circle. Here, the densities of the composite of the 3D models (*red*) are high, because segments A of two 3D models are seen to overlap in this view; in fact, density is at a minimum at this position in the projection map of the multilamellar crystals (*green*). The strongest transmembrane column (2, Fig. 3) is covered by weak densities corresponding to segments B and C in the 3D model (Fig. 4 *a*). The differences appear so large that we must assume very large conformational changes in the membrane region to reconcile these two maps. For example, if we try to fit segment A (Fig. 4 *a*) to the transmembrane column 2, we must assume a shift of 17 Å in the horizontal direction.

Structural differences in the cytoplasmic region

The correlation function between two structures is dominated by the overlap of regions of high density or high contrast. The contrast is high in the cytoplasmic region, whereas densities are high in the transmembrane region. Therefore, if the cytoplasmic domains had moved with respect to the membrane region, the correlation function would provide a compromise and the matching of densities could be poor everywhere. This seems to be the case, because even the densities in the cytoplasmic region do not match well. Hence, to see reorganizations in different regions and domain movements, we must calculate the correlation function based on one region at a time.

To do so, the calculations must begin with the side views, instead of the top views. The 3D model was first rotated by various degrees around an axis perpendicular to the membrane; then it was projected in the direction parallel to the membrane and correlated with the side view of the multi-

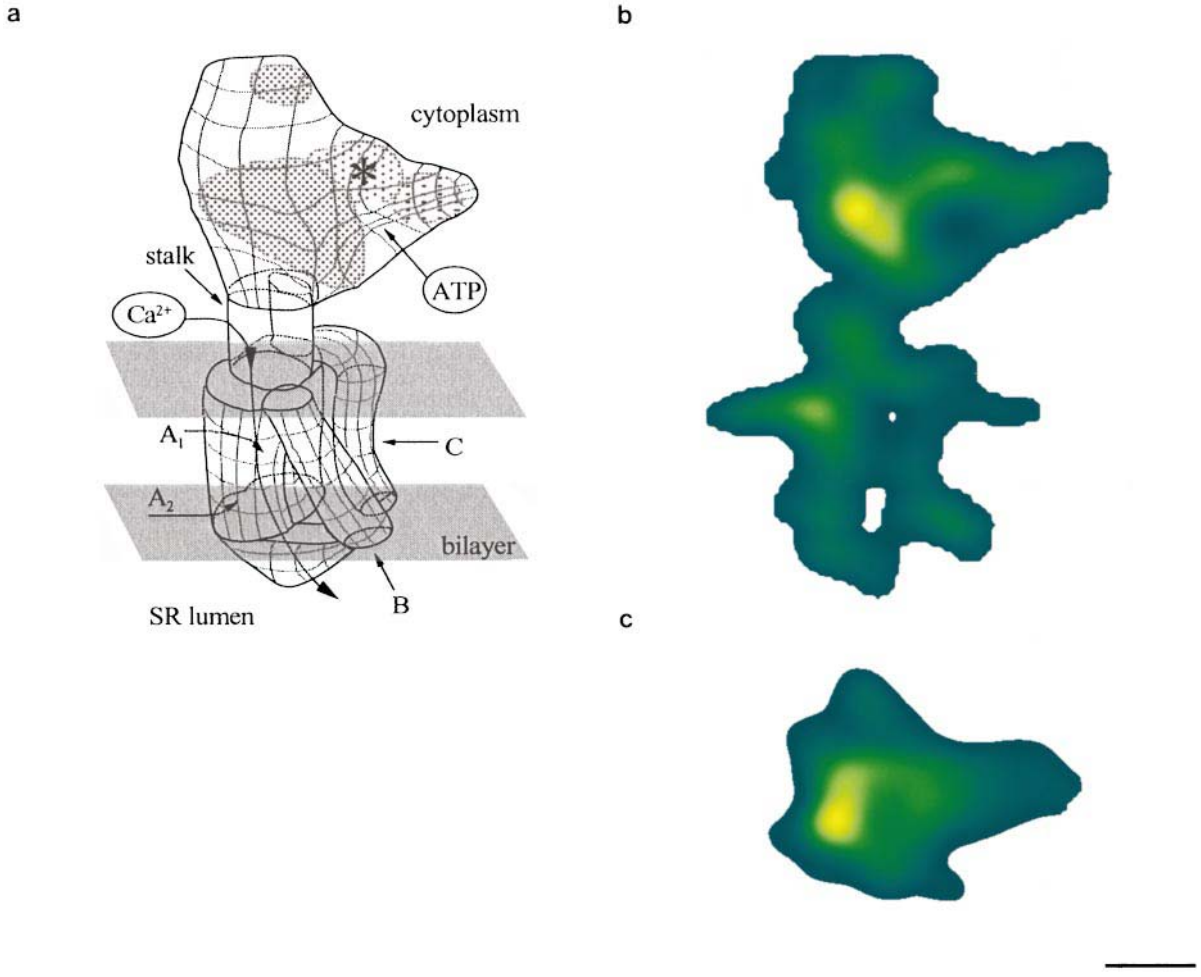

FIGURE 4 (*a*) A cartoon illustrating the structure of Ca^{2+}-ATPase in the absence of calcium. The large cytoplasmic domain looks like the head of a bird; the transmembrane domain has three segments (A, B, and C); the small lumenal domain bridges segments A and B. The proposed ATP binding site and ion pathway are indicated. The asterisk denotes the connecting density in the cytoplasmic domain (see Fig. 7). (*b*) A monomer of Ca^{2+}-ATPase cut from the three-dimensional model of tubular crystals (Toyoshima et al., 1993a) and projected parallel to the plane of the lipid bilayer. (*c*) A projection normal to the lipid bilayer of a monomer cut from the model of tubular crystals. The scale bar corresponds to 20 Å.

lamellar crystals, using only the transmembrane or the cytoplasmic regions. For either of the two regions, the correlation function showed a well-defined peak and reached a maximum when the 3D model (Fig. 4) was rotated clockwise by 11°. The images in Fig. 6, *a* and *b*, are composites of the 3D models superimposed on the side view of the multilamellar crystals at the best matching positions for the cytoplasmic (*a*) and the transmembrane (*b*) regions, respectively.

When the correlation was maximized for only the cytoplasmic region, the larger cytoplasmic domain (HL) was completely covered by the main body of the headpiece of the 3D model (Fig. 6 *a*). The density peaks in the two maps coincided very well. The smaller cytoplasmic domain (HS) was located slightly below the "beak" of the 3D model (Fig. 6 *a*), but the density and the dimensions were similar. The largest change occurred around the groove in the headpiece (Fig. 4 *a*), identified as the ATP binding pocket (Toyoshima et al., 1993a; Yonekura et al., 1997).

Presumably the most interesting feature to note here is the location of the stalk. The positions in the two maps are offset by ~20 Å. In the 3D model (*red*), its position is just beneath the density peak of the headpiece, thus giving an impression that the stalk is offset to the left of the head. In contrast, in the multilamellar crystals, it is offset to the right of the HL domain.

The overall matching of densities was poor, because the transmembrane densities of the 3D model were concentrated on the density minimum in the map of multilamellar crystals (marked by the *open circle* in Fig. 6 *a*). As a result, a large space was left completely uncovered between adjacent enzyme molecules.

Structural differences in the membrane region

When the correlation function was calculated using the transmembrane regions alone, the best matching position

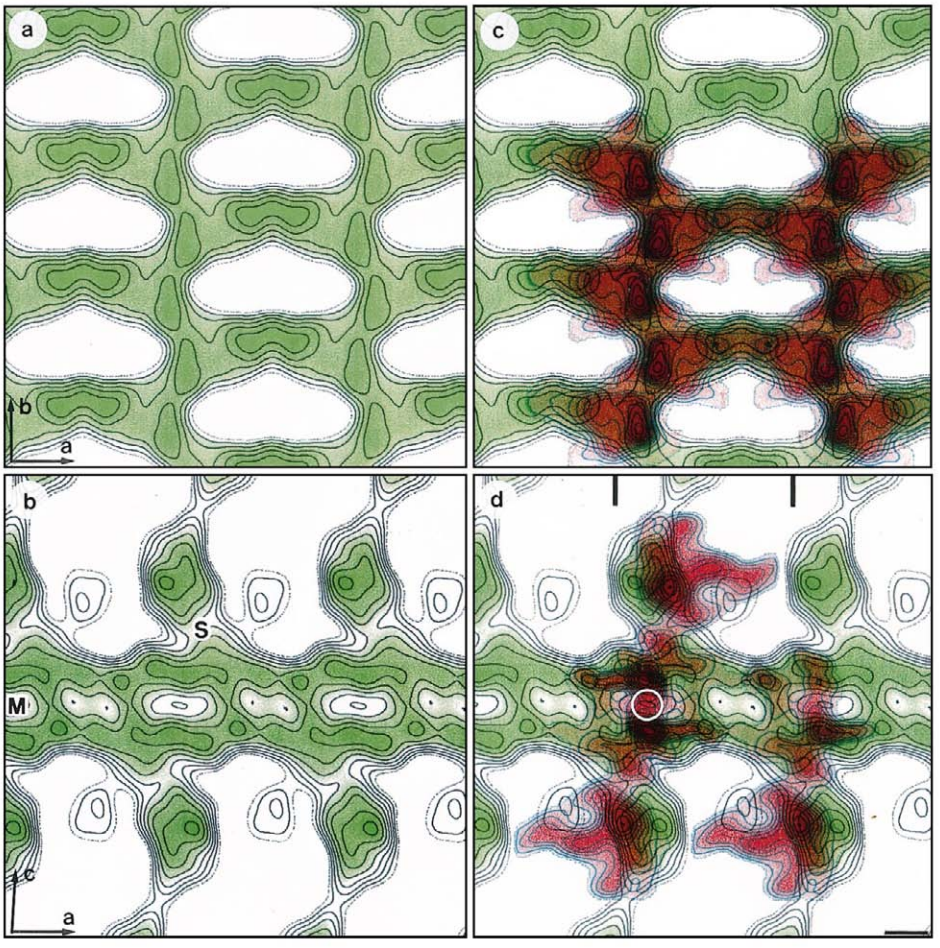

FIGURE 5 (*a*, *b*) Projection maps of multilamellar crystal calculated at 14-Å resolution. (*c*, *d*) Composites of the projection maps at the same resolution of the 3D models from tubular crystals (*red*) and that of multilamellar crystal (*green*), superimposed to maximize the overlap of protein densities. The direction of view is perpendicular to the membrane (*a, c*) or parallel to the plane of the membrane (*b* axis of the multilamellar crystals) (*b, d*). Overlap of densities for the 3D models is correctly reproduced only between the short vertical bars (*d*). The 3D models are located at the best fitting positions, based on the correlation calculation using the top view. Here the 3D models are rotated by 4° counterclockwise from that in Fig. 4 around an axis normal to the membrane. Note that mismatching of density is pronounced around the position marked by the open circle. The transmembrane region (M), the stalk region (S), and the orientation of the unit cell are indicated. The scale bar corresponds to 20 Å.

(Fig. 6 *b*) was shifted slightly (4 Å horizontally) from the position derived from using the whole molecule (Fig. 5 *d*). The correlation function at this position was 77.6%, whereas the correlation function at the best matching position for the whole molecule was 76.8%. The difference was small between these two positions (<1%). However, the fitting in the transmembrane region was significantly better. In particular, the density minimum (*open circle* in Fig. 6 *b*) in the multilamellar crystals (*green*) was bracketed by segments A of neighboring molecules (*red*). Yet the transmembrane column 2 did not coincide exactly with segment A, but was located between segments A and B. Therefore, if we try to match the largest transmembrane segment A in the 3D model to the strongest transmembrane column 2, we must assume a shift of at least 10 Å in the horizontal direction or an inclination of 30° of segment A. In that case, the major part of the cytoplasmic domain will be offset by 20 Å.

DISCUSSION

In this paper we have described a view parallel to the lipid bilayer of the multilamellar crystals of Ca^{2+}-ATPase. The enzyme in this crystal, formed in 10 mM Ca^{2+} at pH 6, must be in a physiological state that is different from that in the tubular crystals formed in the absence of Ca^{2+} (Dux et al., 1987; Stokes and Lacapère, 1994). A quantitative comparison between the projection maps of the enzyme has revealed large conformational differences between the two types of crystals. The most conspicuous difference is observed around the ATP-binding site in the cytoplasmic domain. Because calcium ions are thought to bind directly to the high-affinity sites located in the transmembrane segments (Clarke et al., 1990; Chen et al., 1996), it is surprising to see such large conformational differences in the cytoplasmic region. Of course, we expected to see some conformational changes in the cytoplasmic region, because the binding of calcium must alter the structure around the ATP-binding site, causing hydrolysis of ATP and phosphorylation of the enzyme. Indeed, long-range structural changes have been shown to occur with flash photolysis of caged-calcium (DeLong and Blasie, 1993). Yet the differences are so large and are not localized to a particular part of the enzyme, as demonstrated by the correlation calculations. This suggests that calcium binding elicits dramatic global effects on Ca^{2+}-ATPase structure, resulting in domain rearrangements and segmental movements.

How can the changes in the cytoplasmic domain be interpreted?

The most conspicuous feature in the projection map of the multilamellar crystals is that the cytoplasmic domain con-

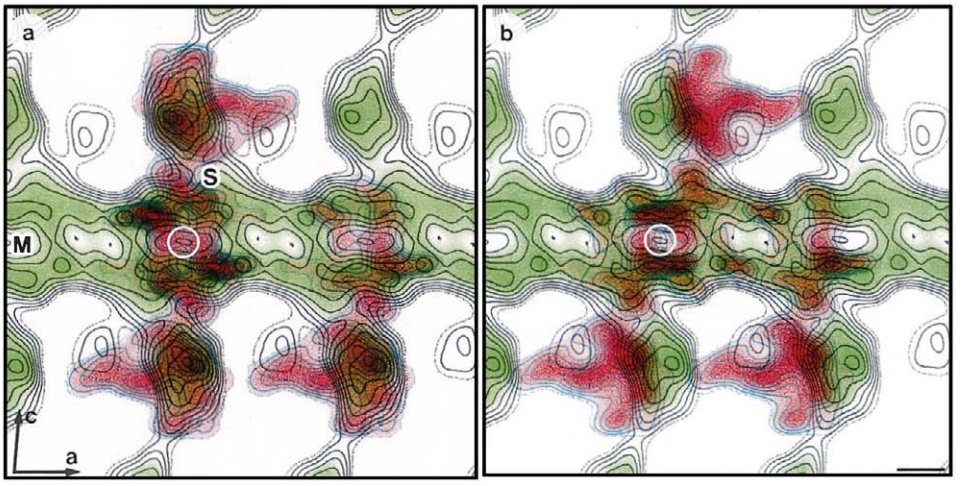

FIGURE 6 Composites of the projection maps of the 3D models from tubular crystals (*red*) and that of multilamellar crystal (*green*), superimposed to maximize the overlap of protein densities in the cytoplasmic (*a*) and transmembrane (*b*) regions. The direction of view is along the plane of the membrane (*b* axis of the multilamellar crystals). The correlation calculations for locating the 3D models used only the cytoplasmic (*a*) or the transmembrane (*b*) region after the 3D model was rotated (Fig. 4) by various degrees around an axis normal to the membrane. For either region, the best fit was obtained when the 3D model was rotated by 11° clockwise. All of the projection maps were calculated at the same resolution (14 Å). The transmembrane region (M), the stalk region (S), and the orientation of the unit cell are indicated. The scale bar corresponds to 20 Å.

sists of two well-separated densities (HL and HS, Fig. 3). This feature can be explained if we assume a movement of the segment connecting the beak and the main body of the cytoplasmic headpiece in the 3D model (Fig. 4 *b*). In this interpretation, as illustrated in Fig. 7, the beak in the 3D model corresponds to the HS domain, and the connecting segment (*asterisk* in Fig. 4 *a*) has moved to form the second density peak closer to the HS domain (*asterisk* in Fig. 3) in

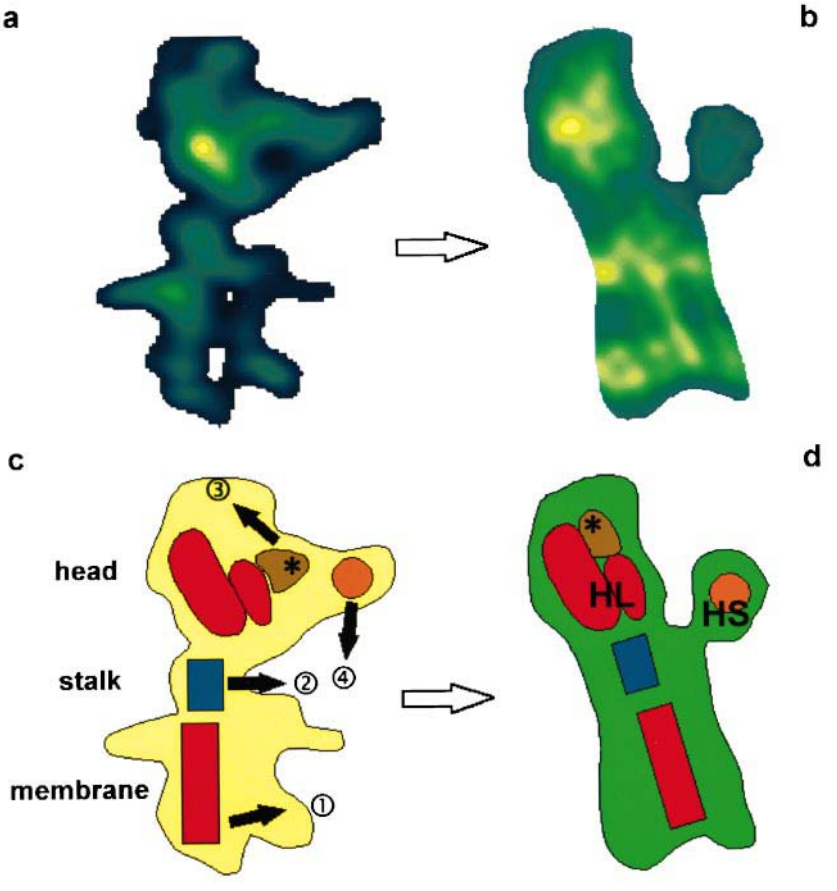

FIGURE 7 A cartoon illustrating the proposed movements in the Ca^{2+}-ATPase caused by the binding of calcium. (*a*) A monomer of Ca^{2+}-ATPase cut from the three-dimensional model of tubular crystals formed in the absence of calcium (identical to Fig. 4 *b*). (*b*) A monomer of Ca^{2+}-ATPase in the multilamellar crystals formed in the presence of calcium, cut from the projection map shown in Fig. 3. (*c*, *d*) Four segments rearranged by the binding of calcium. Arrows indicate the directions of the movements and numbers the order of the segmental movements. Because the best fit of the 3D model was obtained at the same azimuthal position for either the cytoplasmic or the membrane region (Fig. 6), the movements depicted are solely translational ones. The asterisk in the HL domain (*d*) refers to a subsidiary peak that might correspond to the connecting density (*asterisk in c*) in the 3D model (*a, c*).

the HL domain (also see Fig. 6 *b*). Supporting this interpretation, the main body of the cytoplasmic headpiece in the 3D model has only one density peak offset to the left (Fig. 4 *b*). In an 8-Å resolution map of the tubular crystals with bound chromium ATP (Yonekura and Toyoshima, unpublished observations), the beak forms a domain that is distinct from the main body of the headpiece.

It is interesting that such a large change occurs around the putative ATP binding site (Fig. 4 *a*; Toyoshima et al., 1993a; Yonekura et al., 1997), because Ca^{2+}-ATPase in the multilamellar crystals cannot hydrolyze ATP (data not shown). The crystallization medium contains 10 mM Ca^{2+}, which is high enough to inhibit the ATPase activity (Hasselbach, 1964; MacLennan et al., 1972). The crystals put in the assay medium containing 0.15 mM Ca^{2+} exhibited no ATPase activity, even after 10 min of incubation. However, the addition of detergent, which breaks up the crystals, restored full ATPase activity (data not shown). Hence constraints posed by forming a crystal may explain the loss of ATPase activity. Nonetheless, the split appearance of the cytoplasmic domains must not be caused by the crystal contacts between the enzyme molecules in adjacent layers of two-dimensional sheets, because the same density distribution was found for the molecules in the uppermost layer (image not shown).

How the binding signal of calcium is transmitted to the cytoplasmic side

The stalk region must have an important role in transmitting the binding signal of calcium to the ATP-binding site, because the stalk is the only connection between the transmembrane segments and the headpiece of the cytoplasmic domain. In this regard, it may be important to note that the position of the stalk with respect to the headpiece is different between the two structures: in the tubular crystals, the stalk is offset to the left from the center of the headpiece (Fig. 4 *b*); it is offset to the right of the HL domain in the multilamellar crystals (Fig. 3). Furthermore, transmembrane column 2, which appears to be connected to the stalk directly in the projection map of multilamellar crystals, is inclined by 30° from vertical, whereas segment A_1, which is a direct extension of the stalk in the tubular crystals, runs normal to the membrane plane. Thus the binding of calcium might cause the rearrangement of the transmembrane segments, which in turn move the stalk to transmit the binding signal to the cytoplasmic domains (depicted in Fig. 7, *c* and *d*).

Rearrangements of the transmembrane segments

The differences in the transmembrane region are perplexingly large between the two maps, as demonstrated by the poor matching in Fig. 6 *b*, where the correlation of densities in the transmembrane region was maximized. The differences are also difficult to interpret. As already described, the transmembrane region of the enzyme in the tubular crystals consists of three segments; the largest one is segment A. The largest transmembrane segment is column 2 in the multilamellar crystals (Fig. 3). However, column 2 and segment A were not at the same position when the correlation in the transmembrane region was maximized (Fig. 6 *b*). Moreover, in the tubular crystals, there is a lumenal density connecting segments B and A_2; such densities exist, if at all, only in the left side of column 2 in the multilamellar crystals (Fig. 3). In terms of the size and the connectivity to the stalk, it seems appropriate to assign column 2 to segment A. Column 1 is unlikely to be either segment B or C, because it is located in the left side of column 2; hence column 1 is most likely to be a part of segment A. These assignments leave column 3, which will then correspond to segments B and C.

To explain the mismatch of the positions of column 2 and segment A solely by translational movements, segment A must move 13 Å horizontally (Fig. 6 *b*). Nonetheless, a 30° change in the inclination of transmembrane columns (depicted in Fig. 7 *c*) would account for a 10-Å displacement. Therefore, it seems possible to reconcile the two maps, but here again, we are forced to assume large conformational changes to explain the differences.

Conformational states of Ca^{2+}-ATPase in the two forms of crystals

How are the structural differences of the enzyme visualized here between the two crystal forms related to the reaction cycle of Ca^{2+}-ATPase? It is not obvious, because either type of crystal is formed in rather special ionic conditions: tubular crystals are formed in the presence of EGTA and decavanadate, whereas the multilamellar crystals described here are formed in the presence of 10 mM calcium. Several attempts have already been made to address this issue (Dux et al., 1987; Stokes and Lacapère, 1994).

Because of the absence of calcium ions, Ca^{2+}-ATPase in the tubular crystals has been thought to take a conformation after transfer of calcium ions to the lumenal side of the SR (Dux and Martonosi, 1983). Limited proteolysis supports this idea (Imamura et al., 1984). However, further specification is difficult, because vanadate is used for inducing crystals. Decavanadate has been thought to be responsible for crystal formation: in fact, strong density peaks that are likely to represent large vanadate oligomers are observed in the map of tubular crystals (Toyoshima et al., 1993a). However, stock decavanadate solution inevitably contains other species of oligomers (Csermely et al., 1985) that may modulate the structure of the enzyme in different ways (Coan et al., 1986; Aureliano and Madeira, 1994). Monovanadate has been thought to behave as a phosphate analog (Pick, 1982; Pick and Karlish, 1982), and decavanadate as an ATP analog (Varga et al., 1985; Coan et al., 1986; Ross and McIntosh, 1987). Given these results, further characteriza-

tion is clearly needed to identify the physiological state of the enzyme in the tubular crystals.

The conformational state of the enzyme in the multilamellar crystals is not unambiguous either (Dux et al., 1987). Because this type of crystal is formed in high concentrations of calcium (>0.25 mM at pH 6; Stokes and Lacapère, 1994), the enzyme may be regarded to be in a kind of resting state after a large amount of calcium ion is transferred to the lumen of the SR. The question is whether this state is the same as the one in which only low concentrations of calcium are present (the so-called E_1 state). The apparent dissociation constant of calcium at pH 6 has been measured to be ~7.6 μM, and the Hill coefficient to be ~1.46 (Watanabe et al., 1981). These values mean that 99.4% of the high-affinity binding sites are occupied at 0.25 mM calcium; 0.9 mM is required to fill 99.9% of the binding sites. This number for the dissociation constant is also consistent with the one ($pCa_{1/2}$ 5.15) obtained by the intrinsic tryptophan fluorescence measurements (Guillain et al., 1980). It is well documented that the intrinsic fluorescence of tryptophan residues, nearly entirely on putative transmembrane helices, increases when the calcium concentration is increased. The fluorescence saturates at the millimolar range (Guillan et al., 1980, 1981).

A recent study (Juul et al., 1995) showed that high-affinity calcium binding is impaired after digestion with proteinase K in the presence of 0.3 mM Ca^{2+}, but not in 10 mM Ca^{2+} (at pH 6.5). This result is consistent with the fact that a Ca^{2+} concentration greater than 0.3 mM is required to keep the high-affinity binding sites continuously full. It may explain the result that the long-term stability of Ca^{2+}-ATPase is improved by the presence of millimolar Ca^{2+} (Pikula et al., 1988).

It is well known that ATPase activity of Ca^{2+}-ATPase is completely inhibited at millimolar calcium. From kinetic studies, it is established that the inhibition of ATPase activity by a high concentration of calcium is due to the stabilization of the E-P state (Yamada and Ikemoto, 1980), caused by the activation of back-reaction (Trotta and de Meis, 1978). Thus the enzyme in high Ca^{2+} concentrations retains the ability to proceed to the next steps (i.e., binding of ATP and phosphorylation) in the reaction cycle.

The conformational changes accompanying the Ca^{2+} binding to the high-affinity sites have been studied using profile x-ray diffraction of stacked lamellar vesicles (DeLong and Blasie, 1993). They detected conformational changes in three different parts of the enzyme on the release of calcium by flash photolysis of caged calcium. The changes in the projected electron densities were small; the increase in the membrane domain could be attributed to the binding of Ca^{2+} alone, but was accompanied by decreases in the adjacent area. The small size of the changes might appear to be incompatible with the current results. However, the differences in conformation visualized here (Fig. 6) are mostly the movements parallel to the membrane plane, causing little net mass movement normal to the membrane. The mass movements in the headpiece they describe (i.e., the decrease at the top part and the increase at ~15 Å below it) are certainly consistent with the differences depicted in Fig. 7.

Given these results, it seems most appropriate to assume that the enzyme in the multilamellar crystals is in a state similar to, if not identical with, the $E_1 \cdot Ca_2$ state obtained transiently at physiological Ca^{2+} concentrations, which is similar to the conclusion of previous studies (Stokes and Lacapère, 1994).

CONCLUSIONS AND PROSPECTS

Conformational differences between the Ca^{2+}-ATPase in the multilamellar crystals and that in the tubular crystals were unexpectedly large, as visualized in the projection maps viewed parallel to the lipid bilayer. These conformational differences most likely represent the changes triggered by the binding of calcium ions to the high-affinity binding sites within the membrane. The binding signal seems to be realized as the rearrangements of the transmembrane segments and transmitted to the cytoplasmic domain through the change in inclination of the stalk segment, as illustrated in Fig. 7 *c*. Large changes around the putative ATP binding site may be largely accounted for by segmental movements of the cytoplasmic domains.

Of course, these structural differences would be much better characterized and understood if the three-dimensional structure of the multilamellar crystals were available. It is now possible to obtain large, flat crystals that diffract to 3.6-Å resolution by electron diffraction (Shi et al., 1995). At this resolution, it may be feasible to visualize individual amino acids. Thus, in the near future, we may be able to understand the structural changes that are involved in the active transport of calcium ions.

We thank Dr. Nigel Unwin for reading through an initial draft. We also thank Kazutoshi Tani for some of the programs used in this study.

This work was supported by Grants-in-Aid for Scientific Research and for International Scientific Research from the Ministry of Education, Science, Sports and Culture of Japan (to CT) and from the National Institutes of Health (AR40997 to DLS).

REFERENCES

Amos, L. A., R. Henderson, and P. N. T. Unwin. 1982. Three-dimensional structure determination by electron microscopy of two-dimensional crystals. *Prog. Biophys. Mol. Biol.* 39:183–231.

Anderson, K. W., and A. J. Murphy. 1983. Alterations in the structure of the ribose moiety of ATP reduce its effectiveness as a substrate for the sarcoplasmic reticulum ATPase. *J. Biol. Chem.* 258:14276–14278.

Aureliano, M., and V. M. C. Madeira. 1994. Interactions of vanadate oligomers with sarcoplasmic reticulum Ca^{2+}-ATPase. *Biochim. Biophys. Acta.* 1221:259–271.

Bigelow, D. J., and G. Inesi. 1992. Contributions of chemical derivatization and spectroscopic studies to the characterization of the Ca^{2+} transport ATPase of sarcoplasmic reticulum. *Biochim. Biophys. Acta.* 1113: 323–338.

Brandl, C. J., N. M. Green, B. Korczak, and D. H. MacLennan. 1986. Two Ca^{2+}-ATPase genes: homologies and mechanistic implications of deduced amino acid sequences. *Cell.* 44:597–607.

Caspar, D. L. D., C. Cohen, and W. Longley. 1969. Tropomyosin: crystal structure, polymorphism and molecular interactions. *J. Mol. Biol.* 41: 87–107.

Champeil, P., S. Büschlen-Boucly, F. Bastide, and C. Gary-Bobo. 1978. Sarcoplasmic reticulum ATPase. Spin labeling detection of ligand-induced changes in the relative reactivities of certain sulfhydryl groups. *J. Biol. Chem.* 253:1179–1186.

Chen, L., C. Sumbilla, D. Lewis, L. Zhong, C. Strock, M. E. Kirtley, and G. Inesi. 1996. Short and long range functions of amino acids in the transmembrane region of the sarcoplasmic reticulum ATPase. *J. Biol. Chem.* 271:10745–10752.

Cheong, G. W., H. S. Young, H. Ogawa, C. Toyoshima, and D. L. Stokes. 1996. Lamellar stacking in three-dimensional crystals of Ca^{2+}-ATPase from sarcoplasmic reticulum. *Biophys. J.* 70:1689–1699.

Clarke, D. M., T. W. Loo, and D. H. MacLennan. 1990. Functional consequences of alterations to polar amino acids located in the transmembrane domain of the Ca^{2+}-ATPase of sarcoplasmic reticulum. *J. Biol. Chem.* 265:22223–22227.

Coan, C., D. J. Scales, and A. J. Murphy. 1986. Oligovanadate binding to sarcoplasmic reticulum ATPase. *J. Biol. Chem.* 261:10394–10403.

Coll, R. J., and A. J. Murphy. 1984. Purification of the CaATPase of sarcoplasmic reticulum by affinity chromatography. *J. Biol. Chem.* 259: 14249–14254.

Csermely, P., C. Katopis, B. A. Wallace, and A. Martonosi. 1987. The $E_1 \rightarrow E_2$ transition of Ca^{2+}-transporting ATPase in sarcoplasmic reticulum occurs without major changes in secondary structure. *Biochem. J.* 241: 663–669.

Csermely, P., S. Varga, and A. Martonosi. 1985. Competition between decavanadate and fluorescein isothiocyanate on the Ca^{2+}-ATPase of sarcoplasmic reticulum. *Eur. J. Biochem.* 150:455–460.

DeLong, L. J., and J. K. Blasie. 1993. Effect of Ca^{2+} binding on the profile structure of the sarcoplasmic reticulum membrane using time-resolved x-ray diffraction. *Biophys. J* 64:1750–1759.

Downing, K. H., and D. A. Grano. 1982. Analysis of photographic emulsions for electron microscopy of two-dimensional crystalline specimens. *Ultramicroscopy.* 7:381–404.

Dux, L., and A. Martonosi. 1983. Two-dimensional arrays of proteins in sarcoplasmic reticulum and purified Ca^{2+}-ATPase vesicles treated with vanadate. *J. Biol. Chem.* 258:2599–2603.

Dux, L., S. Pikula, N. Mullner, and A. Martonosi. 1987. Crystallization of Ca^{2+}-ATPase in detergent-solubilized sarcoplasmic reticulum. *J. Biol. Chem.* 262:6439–6442.

Dux, L., K. A. Taylor, H. P. Ting-Beall, and A. Martonosi. 1985. Crystallization of the Ca^{2+}-ATPase of sarcoplasmic reticulum by calcium and lanthanide ions. *J. Biol. Chem.* 260:11730–11743.

Girardet, J-L., and Y. Dupont. 1992. Ellipticity changes of the sarcoplasmic reticulum Ca^{2+}-ATPase induced by cation binding and phosphorylation. *FEBS Lett.* 296:103–106.

Guillain, F., P. Champeil, J-J. Lacapère, and M. P. Gingold. 1981. Stopped flow and rapid quenching measurement of the transient steps induced by calcium binding to sarcoplasmic reticulum adenosine triphosphatase. Competition with Ca^{2+}-independent phosphorylation. *J. Biol. Chem.* 256:6140–6147.

Guillain, F., M. P. Gingold, S. Büschlen, and P. Champeil. 1980. A direct fluorescence study of the transient steps induced by calcium binding to sarcoplasmic reticulum ATPase. *J. Biol. Chem.* 255:2072–2076.

Hasselbach, W. 1964. Relaxing factor and the relaxation of muscle. *Prog. Biophys. Biophys. Chem.* 14:169–222.

Henderson, R., J. M. Baldwin, K. H. Downing, J. Lepault, and F. Zemlin. 1986. Structure of purple membrane from *Halobacterium halobium*: recording, measurement and evaluation of electron micrographs at 3.5 Å resolution. *Ultramicroscopy.* 19:147–178.

Imamura, Y., K. Saito, and M. Kawakita. 1984. Conformational change of Ca^{2+},Mg^{2+}-adenosine triphosphatase of sarcoplsmic reticulum upon binding of Ca^{2+} and adenyl-5′-yl-imidodiphosphate as detected by trypsin sensitivity analysis. *J. Biochem.* 95:1305–1313.

Inesi, G. 1994. Teaching active transport at the turn of the twenty-first century: recent discoveries and conceptual changes. *Biophys. J.* 66: 554–560.

Juul, B., H. Turc, M. L. Durand, A. G. de Gracia, L. Denoroy, J. V. Møller, P. Champeil, and M. le Maire. 1995. Do transmembrane segments in proteolyzed sarcoplasmic reticulum Ca^{2+}-ATPase retain their functional Ca^{2+} binding properties after removal of cytoplasmic fragments by proteinase K? *J. Biol. Chem.* 270:20123–20134.

MacLennan, D. H., C. J. Brandl, B. Korczak, and N. M. Green. 1985. Amino-acid sequence of a Ca^{2+} + Mg^{2+}-dependent ATPase from rabbit muscle sarcoplasmic reticulum, deduced from its complementary DNA sequence. *Nature*. 316:696–700.

MacLennan, D. H., C. C. Yip, G. H. Iles, and P. Seeman. 1972. Isolation of sarcoplasmic reticulum proteins. *Cold Spring Harb. Symp. Quant. Biol.* 37:469–477.

Martonosi, A. N. 1995. The structure and interactions of Ca^{2+}-ATPase. *Biosci. Rep.* 15:263–281.

Møller, J. V., B. Juul, and M. le Maire. 1996. Structural organization, ion transport, and energy transduction of P-type ATPases. *Biochim. Biophys. Acta.* 1286:1–51.

Nakamoto, R. K., and G. Inesi. 1986. Retention of ellipticity between enzymatic states of the Ca^{2+}-ATPase of sarcoplasmic reticulum. *FEBS. Lett.* 194:258–262.

Pick, U. 1982. The interaction of vanadate ions with the Ca-ATPase from sarcoplasmic reticulum. *J. Biol. Chem.* 257:6111–6119.

Pick, U., and S. J. D. Karlish. 1980. Indications for an oligomeric structure and for conformational changes in sarcoplasmic reticulum Ca^{2+}-ATPase labelled selectively with fluorescein. *Biochem. Biophys. Acta.* 626: 255–261.

Pick, U., and S. J. D. Karlish. 1982. Regulation of the conformation transition in the Ca-ATPase from sarcoplasmic reticulum by pH, temperature, and calcium ions. *J. Biol. Chem.* 257:6120–6126.

Pikula, S., N. Mullner, L. Dux, and A. Martonosi. 1988. Stabilization and crystallization of Ca^{2+}-ATPase in detergent-solubilized sarcoplasmic reticulum. *J. Biol. Chem.* 263:5277–5286.

Rice, W. J., and D. H. MacLennan. 1996. Scanning mutagenesis reveals a similar pattern of mutation sensitivity in transmembrane sequences M4, M5, and M6, but not in M8, of the Ca^{2+}-ATPase of sarcoplasmic reticulum (SERCA1a). *J. Biol. Chem.* 271:31412–31419.

Ross, D. C., and D. B. McIntosh. 1987. Intramolecular cross-linking at the active site of the Ca^{2+}-ATPase of sarcoplasmic reticulum. *J. Biol. Chem.* 262:12977–12983.

Schertler, G. F. X., C. Villa, and R. Henderson. 1993. Projection structure of rhodopsin. *Nature.* 362:770–772.

Shi, D., H-H. Hsiung, R. C. Pace, and D. L. Stokes. 1995. Preparation and analysis of large, flat crystals of Ca^{2+}-ATPase for electron crystallography. *Biophys. J.* 68:1152–1162.

Stokes, D. L., and N. M. Green. 1990a. Structure of Ca-ATPase: electron microscopy of frozen-hydrated crystals at 6 Å resolution in projection. *J. Mol. Biol.* 213:529–538.

Stokes, D. L., and N. M. Green. 1990b. Three-dimensional crystals of Ca-ATPase from sarcoplasmic reticulum. *Biophys. J.* 57:1–14.

Stokes, D. L., and J. J. Lacapère. 1994. Conformation of Ca^{2+}-ATPase in two crystal forms. *J. Biol. Chem.* 269:11606–11613.

Tani, K., H. Sasabe, and C. Toyoshima. 1996. A set of programs for determining defocus and astigmatism in electron images. *Ultramicroscopy.* 65:31–44.

Taylor, K. A., N. Mullner, S. Pikula, L. Dux, C. Peracchia, S. Varga, and A. Martonosi. 1988. Electron microscope observations on Ca^{2+}-ATPase microcrystals in detergent-solubilized sarcoplasmic reticulum. *J. Biol. Chem.* 263:5287–5294.

Taylor, W. R., and N. M. Green. 1989. The predicted secondary structures of the nucleotide-binding sites of six cation-transporting ATPases lead to a probable tertiary fold. *Eur. J. Biochem.* 179:241–248.

Toyoshima, C. 1989. On the use of holey grids in electron crystallography. *Ultramicroscopy.* 30:439–444.

Toyoshima, C., H. Sasabe, and D. L. Stokes. 1993a. Three-dimensional cryo-electron microscopy of the calcium ion pump in the sarcoplasmic reticulum membrane. *Nature.* 362:469–471.

Toyoshima, C., K. Yonekura, and H. Sasabe. 1993b. Contrast transfer for frozen-hydrated specimens. II. Amplitude contrast at very low frequencies. *Ultramicroscopy.* 48:165–176.

Trotta, E. E., and L. de Meis. 1978. Adenosine 5′-triphosphate-orthophosphate exchange catalyzed by the Ca^{2+}-transport ATPase of brain. *J. Biol. Chem.* 253:7821–7825.

Varga, S., P. Csermely, and A. Martonosi. 1985. The binding of vanadium (V) oligoanions to sarcoplasmic reticulum. *Eur. J. Biochem.* 148: 119–126.

Watanabe, T., D. Lewis, R. Nakamoto, M. Kurzmack, C. Fronticelli, and G. Inesi. 1981. Modulation of calcium binding in sarcoplasmic reticulum adenosinetriphosphatase. *Biochemistry.* 20:6617–6625.

Yamada, S., and N. Ikemoto. 1980. Reaction mechanism of calcium-ATPase of sarcoplasmic reticulum. *J. Biol. Chem.* 255:3108–3119.

Yamamoto, H., Y. Imamura, M. Tagaya, T. Fukui, and M. Kawakita. 1989. Ca^{2+}-dependent conformational change of the ATP-binding site of Ca^{2+}-transporting ATPase of sarcoplasmic reticulum as revealed by an alteration of the target-site specificity of adenosine triphosphopyridoxal. *J. Biochem.* 106:1121–1125.

Yonekura, K., D. L. Stokes, H. Sasabe, and C. Toyoshima. 1997. The ATP-binding site of Ca^{2+}-ATPase revealed by electron image analysis. *Biophys. J.* 72:997–1005.